Journal of Nuclear Materials 408 (2011) 90–95

Contents lists available at ScienceDirect

Journal of Nuclear Materials

journal homepage: www.elsevier.com/locate/jnucmat

# Creep behaviour of δ-phase of U–Zr system by impression creep technique

T.R.G. Kutty [a,*], C.B. Basak [b], Arun Kumar [a], H.S. Kamath [c]

[a] Radiometallurgy Division, Bhabha Atomic Research Centre, Mumbai 400 085, India
[b] Materials Science Division, Bhabha Atomic Research Centre, Mumbai 400 085, India
[c] Nuclear Fuels Group, Bhabha Atomic Research Centre, Mumbai 400 085, India

ARTICLE INFO

*Article history:*
Received 20 April 2010
Accepted 8 November 2010

ABSTRACT

In this study, the impression creep behaviour of δ-phase of U–50 wt.% Zr (U–72.29 at.% Zr) system was studied in the temperature range 525–575 °C at different stresses. The velocity of the punch at different stresses and temperatures were evaluated for the above alloy. The stress exponents and thermal activation parameters of the above alloy were determined. A power law behaviour is displayed with the stress exponents range from 6.5 to 7. The activation enthalpy for the δ-$UZr_2$ was found to be independent of stress with an average value of 106 kJ/mol.



## 1. Introduction

In the U–Zr system, the composition of the intermediate phase, δ, could be approximated as $UZr_2$ [1,2]. The δ-phase is formed by either an eutectoid or a peritectoid reaction. The peritectoid reaction (α-U) + $\gamma_2 \leftrightarrow \delta$ occurs at 617 °C and 63 at.% Zr, and that the eutectoid reaction $\gamma_2 \leftrightarrow$ (α-Zr) + δ occurs at 606 °C and 76 at.% Zr [3]. Homogeneity range and crystal structure of the intermediate δ-phase in the U–Zr alloy have been studied by electron probe microanalysis, X-ray diffraction and differential thermal analysis, using the alloys prepared by arc-melting. The homogeneity range of the δ-phase was found to be 64.2–78.2 at.% Zr at 600 °C and 66.5–80.2 at.% Zr at 550 °C [4]. The Zr-rich boundary extends toward Zr-rich regions at lower temperatures. Its structure appears to be unique being as a modified C32 ($AlB_2$-type) structure like the so-called ω phase, which is a metastable phase present in Zr-based alloys. The Al position is preferentially occupied by Zr and the B position by a random mixture of U and Zr [3–10]. Little data exists in the literature for the properties of δ-$UZr_2$. The aim of this study is to evaluate the mechanical properties like creep of the above which will be useful for the nuclear community.

Metallic fuels such as U–Zr and U–Pu–Zr alloys are being considered as nuclear fuels for sodium-cooled fast reactors due to their excellent thermal conductivities, high densities and good breeding performance. In fast reactors, the clad operates at high peak clad temperature (~600 °C) in the environment of fast neutron flux (>$10^{15}$ n/$cm^2$) and stresses (~100 MPa). In this aggressive environment, various thermo-mechanical phenomena such as clad thermal and irradiation creep, void swelling and fuel–clad mechanical interaction may limit the achievable burnup. Therefore, predicting the behaviour of the fuel is very important objective in fast reactors design and analysis [11–13].

The temperature gradient observed in a metallic fuel may create two temperature regions; above and below 606 °C which is the temperature range for a phase transformation ($\gamma_2 \leftrightarrow$ α-Zr + δ-$UZr_2$). At the beginning of irradiation, most of the fuel is in the α + δ-phase field with only the hottest part of the fuel in the high temperature $\gamma_1 + \gamma_2$ or γ field [14,15]. For a typical fuel pin, the metal fuel slug undergoes significant swelling upon irradiation, due to the generation of the fission gases. Fuel–clad contact occurs within 1–2 at.% peak burnup. The data show that prior to making contact with the cladding tube, metallic alloy fuel swells rapidly due to its high fission-enhanced creep rate and irradiation growth [16,17]. A higher swelling implies higher fission-gas diffusivity and higher creep rate in the central region of the fuel. As a result of a higher swelling rate and fluid like behaviour in the hotter central part of the fuel, the fuel in this region is in a hydrostatic stress state, while the cooler and stronger outer shell is in a state of tensile stress. The effect of these tensile stresses on swelling and creep in the outer fuel zone explains the larger radial than axial swelling and, thus, observed anisotropy in swelling. The outer, anisotropic swelling leads to large radial cracks, presumably because there is insufficient time to relax radial stresses by means of creep [14].

Also, it may be noted that the fuel and clad get 'locked' both axially and radially, in the upper section of the fuel. The fuel in this region is in γ-phase and rather compliant. It could be possible to control the thermal creep of the fuel by only adjusting the gas plenum height [14]. On the other hand, the middle and lower regions of the fuel along the axis are colder and stiffer. (α + δ) phase fraction is significantly present here. Also, the fuel-cladding contact and thermal gradients would cause the fuel slug to ratchet up the fuel column, further exacerbated by fuel creep during irradiation that would prevent the fuel from dropping to the original po-

* Corresponding author. Tel.: +91 22 25595361; fax: +91 22 25505151.
*E-mail address:* tkutty@barc.gov.in (T.R.G. Kutty).

0022-3115/$ - see front matter © 2010 Elsevier B.V. All rights reserved.
doi:10.1016/j.jnucmat.2010.11.016

sition during shutdown [16]. The concern was that a sudden drop of the fuel slug in the cladding caused by specific reactor operating conditions would result in a sudden reactivity insertion, an obvious safety problem to reactor operation. Furthermore, during transients, one has to guard against fuel/clad chemical interaction (FCCI), which may result in the formation of low-melting eutectics that waste the clad [14,18]. Therefore, any credible attempt at assessing the performance of metal fuel must include models that are able to predict the time-dependent temperature, stress and strain distribution and microstructural evolution within the clad and fuel for given operating and abnormal conditions [14]. These models should include the effects of fission gas release, fuel swelling and creep, FCMI, clad thermal and irradiation creep, fuel restructuring, FCCI and clad failure [19,20]. On account of the information given above, one must know the creep behaviour of the fuel for the smooth operation of the reactor.

Little data exists for the creep behaviour of δ-$UZr_2$. Hence, a study of the creep behaviour of the δ-$UZr_2$ phase as a function of stress, temperature and microstructure is undertaken. Assessment of the thermal creep behaviour would aid in gaining a better understanding of irradiation creep. Furthermore, creep data could be of immense help in understanding the diffusion behaviour. In this paper, the creep behaviour of the δ-$UZr_2$ phase of U–50 wt.% Zr (U–72.29 at.% Zr) system is investigated by the impression creep technique.

## 2. Impression creep

Impression creep technique is a modified indentation creep test wherein the conical or ball indenter is replaced by a cylindrical, flat bottomed punch [21]. A schematic diagram of the impression creep apparatus is shown in Fig. 1. The technique, because of its simplicity, is immensely useful in investigating the creep properties of materials. Li and co-workers [22–25] and Sastry and co-workers [26–29] have applied this test to investigate a number of deformation aspects. In the impression creep test, depth of penetration of the punch at a given stress versus time yields the creep curve. Two steady state velocities were found for indenter, one near the surface and the other deep into the specimen. The former is called "impression creep" and the latter is called "penetration creep" [22]. Since the latter may involve friction between indenter and the specimen, only the former is studied in detail. The high temperature impression curves obtained by Yu and Li [25] and Murthy and Sastry [27] resemble the conventional tensile creep curves in exhibiting a steady state after an initial transient period. The steady state impression velocity of the punch was found to have the same stress and temperature dependence as in the conventional creep. The rate controlling mechanisms of plastic flow in the impression creep and in tensile creep deformation were shown to be same by comparing the activation energy and activation area in the two types of creep [21,22]. It was further shown that the steady state velocity of the punch in impression creep testing varies linearly with punch diameter for the same punching stress [22]. Because the punch geometry is a flat end cylinder, the plastic zone developed beneath the punch assumes a constant size when the punch penetrates into the specimen.

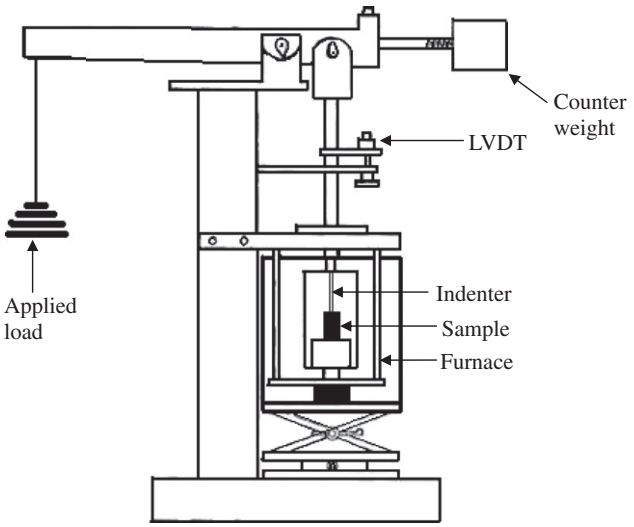


**Fig. 1.** A schematic diagram of impression creep testing apparatus.

The impression creep test is an elegant test technique which offers the following advantages over the conventional creep testing [21]:

1. A small quantity of testing material is sufficient.
2. Constant stress can be obtained with a constant load.
3. The temperature and stress dependence of the steady state (or minimum) creep rate can be obtained on a single specimen.
4. Absence of tertiary stage of creep makes the deformation more stable and the test is, therefore, better suited for investigating near brittle materials.

## 3. Estimation of activation parameters

It can be seen that, as in a conventional creep test, a steady state is reached for the punch velocity after an initial transient period wherein the punch velocity decreases with time. A characteristic parameter describing the high temperature creep is the stress exponent, $n$, for steady-state creep rate in the power-law creep equation. This can be expressed as:

$$n = \Delta \ln \dot{\varepsilon} / \Delta \ln \sigma_t = \Delta \ln v_s / \Delta \ln \sigma_i. \quad (1)$$

where $\dot{\varepsilon}$ (=$d\varepsilon/dt$) is the steady tensile creep rate, $\sigma_t$ is the applied stress in tensile creep test, $v_s$ is the steady state velocity of the punch in impression creep and $\sigma_i$ is the punching stress in impression creep test. The following relationships hold between the stress and strain parameters in the two types of creep [22]:

$$\dot{\varepsilon} = v_s/d \approx v_s/a. \quad (2)$$

$$\sigma_i = 3\sigma_t. \quad (3)$$

In the above equation, $a$ is the diameter of the punch and $d$ is the depth of the plastic zone beneath the punch. The factor 3 involved in the conversion of stresses in Eq. (3) is for an isotropic material like aluminium [21]. It is evident that there is agreement in the $n$ values derived separately from the two types of creep test. The values of activation energy derived from impression creep testing (including those estimated from differential-temperature impression creep testing) agree well with those obtained from tensile creep tests as well as those obtained from plain tensile testing (variation of flow stress with temperature and imposed strain rate). The activation energy can be computed from the following expression [22].

$$Q = -k[\delta \ln v/\delta(1/T)]_{\tau^*} = -k[\delta \ln \dot{\varepsilon}/\delta(1/T)]_{\tau^*}$$
$$\cong -k[\Delta \ln v/\Delta(1/T)]_{\tau} \cong -k[\Delta \ln \dot{\varepsilon}/\Delta(1/T)]_{\tau}. \quad (4)$$

## 4. Experimental

### 4.1. Fabrication of alloy

Buttons of the U–50%Zr (U–72.29 at.% Zr) alloy, weighing about 20 g, were prepared by arc-melting together pure uranium and zir-

conium metals. The purities of starting materials, uranium and zirconium, were 99.9% and 99.95%, respectively. The zirconium metal used in this study was a crystal bar supplied by Nuclear Fuel Complex, Hyderabad. Each alloy button was melted six to eight times to ensure its homogeneity. Oxidation of the ingot during the fabrication was minimized by arc-melting a pure Zr button before each melting cycle. The alloy buttons obtained were sealed in quartz ampoules that had been evacuated at room temperature to about $1 \times 10^{-2}$ Pa and then filled with high-purity argon. The buttons were first homogenized at 800 °C for 24 h and then quenched in water. Finally, each button was isothermally held at different temperatures at the δ-phase field (i.e. 525, 550, and 575 °C), at which creep testing would be done, for 48 h. The composition of the alloy and the impurities present are given in Table 1.

### 4.2. Characterization

X-ray diffraction was performed on the above heat treated alloy buttons to ensure the presence of 100% δ-phase. Diffraction patterns were obtained by the step-scan method with monochromatic Cu Kα radiation, with a step size of 0.008° and a measuring time of 2 s at each step were used. The microstructure was examined by using an optical microscope under polarized light illumination. The microstructure was further examined by using a scanning electron microscope (SEM) for a compositional contrast by using a back scattered electron image. Elemental analyses were made by using an energy dispersive spectroscope (EDS).

For differential thermal analysis (DTA), about 5 mm long samples of alloy were cut using a low-speed cutoff wheel. This sample was then placed into an alumina crucible positioned on the DTA sensor head. During DTA operation, the inside of the DTA furnace was purged with highly purified argon gas flowing at 2 l/min. Rates of heating and cooling were programmed at 10 and 20 °C/min, respectively. The temperature calibration was accomplished by measuring the melting points of high purity metals, such as Zn, Al and Ag. The resulting thermogram was recorded. After the measurement, weight changes of the samples were negligible and their surfaces remained shiny. This indicates that no excessive sample oxidation occurred during the heating/cooling cycles.

### 4.3. Creep testing

The impression creep apparatus used for this study was basically similar to the one described by Yu and Li [25]. The vertical movement of the pull rod and hence the impression depth was sensed through an LVDT transducer. The punch displacement could be measured with an accuracy of ±3 μm. The test samples were 10 mm × 10 mm and of 5 mm height. The experiment was conducted in high vacuum ($10^{-4}$ torr) using 1.5 mm diameter tungsten carbide indenter. The sample was heated to the required temperature and a predetermined load was added and the impression creep curve recorded. The temperature was maintained within ±1 °C. During the impression creep test, a steady state velocity of the punch was reached after an initial transient period. Thereafter, the punching stress was increased and the new creep curve was recorded. The impression creep testing was carried out at 525, 550, and 575 °C. At each temperature, the experiment was conducted at different stresses varying from 12.97 to 37.05 MPa. In all cases, the depth of penetration was limited to a maximum value of 2.0 mm.

## 5. Results

XRD results for the starting alloy are presented in Fig. 2. The data clearly shows the presence of only δ-phase. The microstructure of the above is shown in Fig. 3. Typical impression creep curves, i.e. impression depth versus time curves, are shown in Fig. 4 for alloy at a constant temperature of 525 °C for different stresses varying from 12.97 to 37.05 MPa obtained with a 1.5 mm diameter indenter. In general, the initial primary creep which sometimes extends up to 20 h is followed by a secondary stage. Figs. 5 and 6 shows the creep curves at 550 °C and 575 °C,

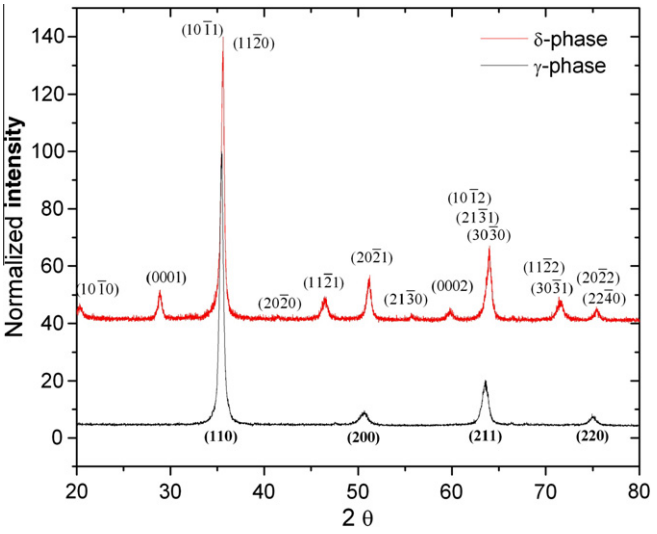


**Fig. 2.** XRD pattern of δ-phase of U–50%Zr alloy. X-ray diffraction pattern confirm the presence of 100% δ-phase. For comparison, XRD pattern of γ-phase is also shown in the same figure.

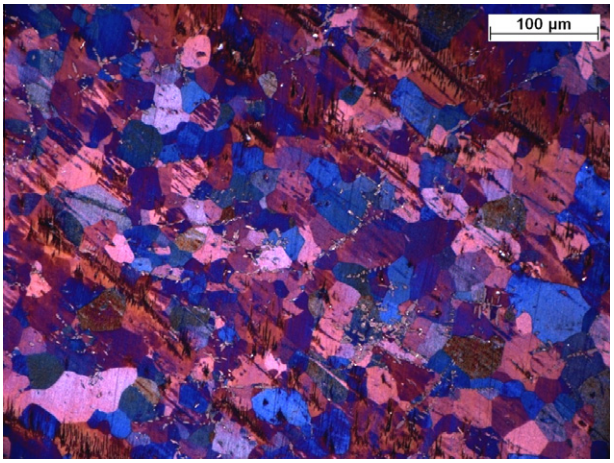


**Fig. 3.** The microstructure of δ-phase of U–50%Zr alloy under polarized light.

**Table 1**
Chemical composition of U–50 wt%Zr (U–72.29 at.% Zr) alloys. Zr and U contents are in wt.%; rests are in ppm.

| Alloy | Zr | U | C | N | O | Y | Fe | Ni | Cr | Mg | Mn | Ce |
|---|---|---|---|---|---|---|---|---|---|---|---|---|
| U–50 wt%Zr | 50.06% | Rest | 450 | 60 | 580 | 204 | 40 | 25 | 4.8 | 16 | 5 | 8.7 |

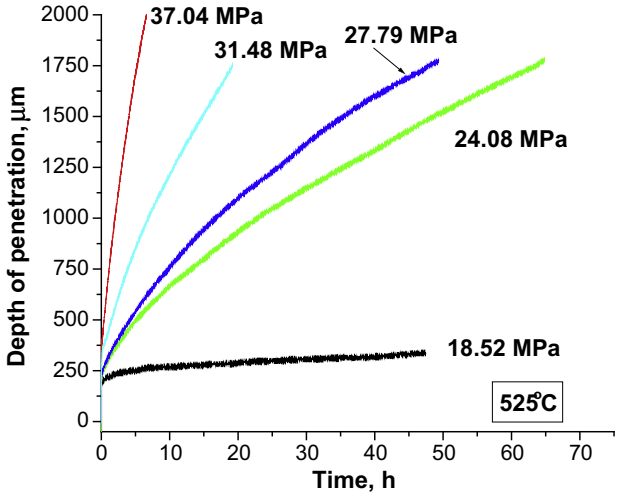


**Fig. 4.** The impression creep curves – the impression depth versus time curves – obtained for U–50%Zr alloy at 525 °C.

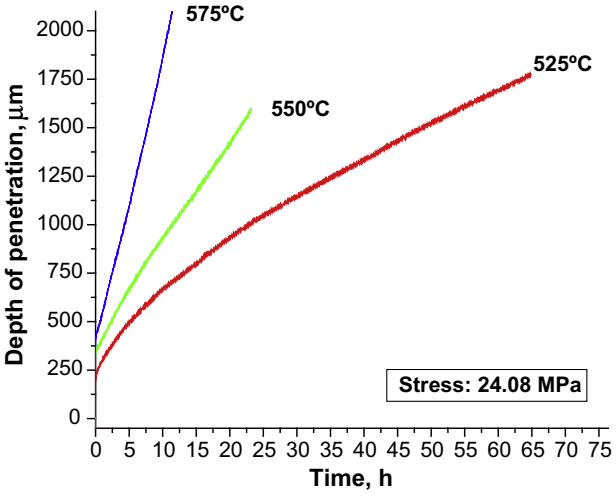


**Fig. 7.** The impression creep curves for a constant stress of 24.08 MPa for different temperatures.

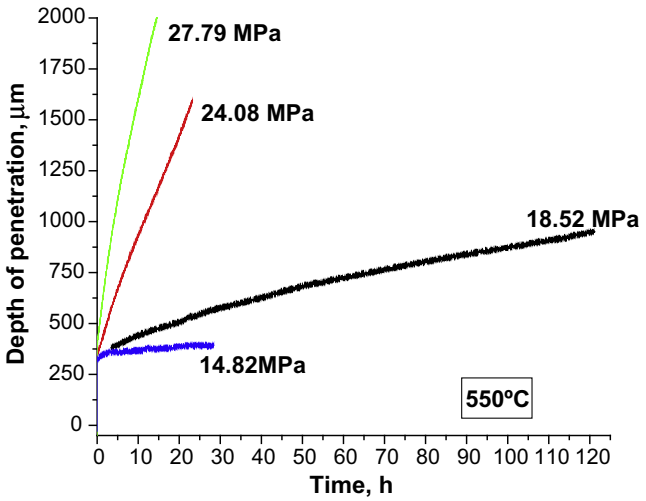


**Fig. 5.** The impression creep curves for U–50%Zr alloy at 550 °C for different stresses.

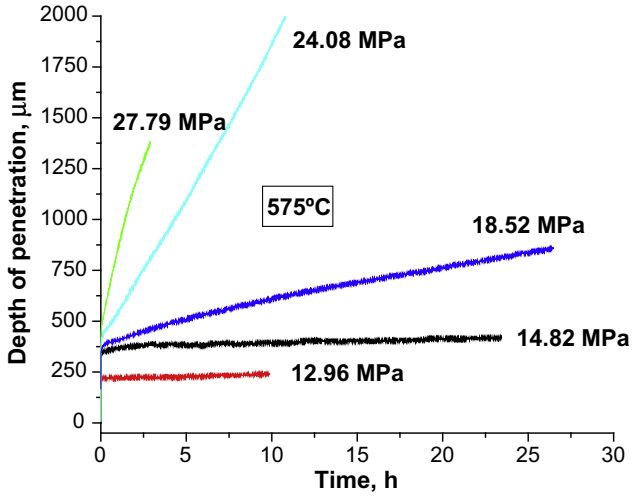


**Fig. 6.** The impression creep curves obtained for U–50%Zr alloy at 575 °C for various stresses.

respectively. Fig. 7 shows the impression creep curves at a constant stress of 24.08 MPa for three different temperatures. It can be seen that, as in conventional creep tests, a steady state (linear portion) is attained for the velocity after an initial transient period during which the penetration of the indenter into the sample surface decreases with time. An interesting feature of the curves in Figs. 4–6 is the absence of the tertiary stage of creep unlike in conventional tensile creep tests. The restriction caused by the rigid (elastic) material which envelopes the plastic zone under the punch is responsible for the absence of the tertiary stage of creep. As a result, the deformation under the cylindrical punch is always stable and therefore the steady state stage is sustained for long periods. This is a unique advantage of the impression creep technique over the unidirectional tensile creep tests.

The slope of the steady state portion of the impression creep curve gives the steady state impression velocity $v$. The impression velocity at 525, 550 and 575 °C for different stresses are given in Table 2. The steady state impression creep rate is plotted in Fig. 8 for U–50%Zr alloy as a function of stress at three different temperatures. A power law with a stress exponent $n$ varying from 6.5 to 7 is seen to be obeyed. The temperature dependence of steady state impression velocity in U–50%Zr alloy is documented in Fig. 9. The computed activation enthalpy values for the above alloy

**Table 2**
Impression velocity at 525, 550 and 575 °C for different stresses.

| Temperature (°C) | Stress (MPa) | Steady state impression velocity (μm/h) | Creep rate ($s^{-1}$) | Stress exponent, $n$ |
|---|---|---|---|---|
| 525 | 18.52 | 1.749 | 3.238E−7 | |
| | 24.08 | 18.225 | 3.375E−6 | |
| | 27.79 | 20.936 | 3.877E−6 | 6.90 |
| | 31.49 | 64.692 | 1.198E−5 | |
| | 37.04 | 267.462 | 4.953E−5 | |
| 550 | 14.82 | 1.603 | 2.968E−7 | |
| | 18.52 | 3.920 | 7.259E−7 | |
| | 24.08 | 49.750 | 9.213E−6 | 6.92 |
| | 27.79 | 93.528 | 1.732E−5 | |
| 575 | 12.97 | 2.946 | 5.455E−7 | |
| | 14.82 | 1.893 | 3.506E−7 | |
| | 18.52 | 14.855 | 2.751E−6 | 6.58 |
| | 24.08 | 152.172 | 2.818E−5 | |
| | 27.79 | 402.732 | 7.458E−5 | |

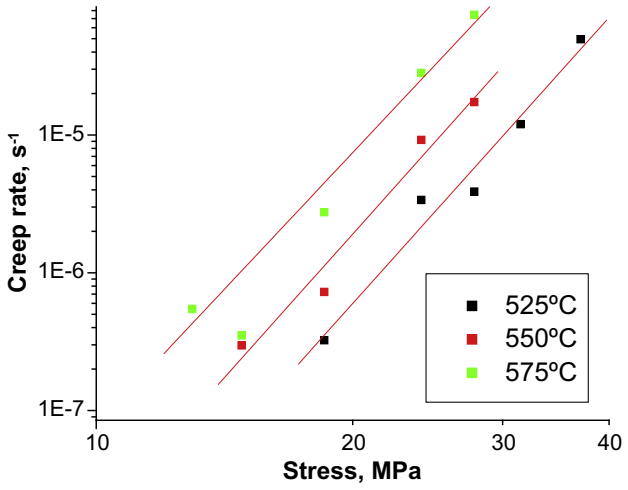


**Fig. 8.** Creep rate versus stress plot in log–log scale for the determination of stress exponent.

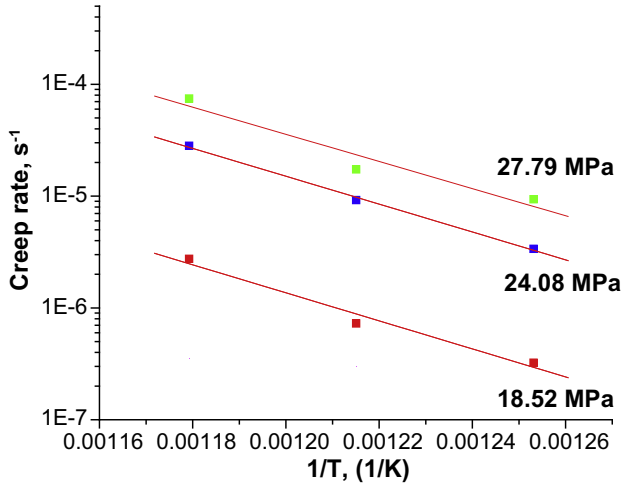


**Fig. 9.** ln ($\varepsilon^{\circ}$) versus ($1/T$) plot for the determination of activation energy for U–50%Zr alloy.

are found to be independent of stress with an average value of 106 ± 4 kJ/mol.

## 6. Discussion

There has been renewed interest in zirconium containing actinide alloys such as U–Zr and U–Pu–Zr as nuclear fuels for fast reactors. The diffusion and creep data and the thermodynamic properties of the above alloys are very important for understanding the phenomena occurring under irradiation [5]. These data are also important in analyzing the fuel behaviour such as redistribution of the components in the temperature gradient under irradiation [6]. Ogata et al. [9] have investigated the interdiffusion behaviour of homogeneous cubic (γ-U, β-Zr) phases in the U–Zr system. A very complete and accurate investigation of diffusion in the U–Zr system was carried out by Adda et al. in the temperature range of 550–1075 °C [30,31]. They observed a minima of the interdiffusion coefficients at composition of $N_{Zr} \sim 0.7$ in the temperature range of 950–1075 °C. The compositions of the minima correspond to those of δ-phase [6]. Akabori et al. have evaluated the apparent diffusion coefficient for δ-phase at 823 and 853 K (550 and 580 °C), which were $0.49 \times 10^{-17}$ and $1.22 \times 10^{-17}$ m$^2$/s, respectively [5]. The activation energy versus concentration plot for U–Zr system showed that the activation energy decreases with Zr concentration and showed a minima at about 30 at.% and then gradually increased with further addition of Zr [30].

As mentioned earlier, during the irradiation of metallic fuel, the constituents redistribute, resulting a microstructure that exhibits three distinct concentric zones; a Zr-enriched central zone (single γ-phase), a Zr-depleted U-enriched intermediate zone (β + γ-phase), and a Zr-enriched zone on the outer periphery (α + δ-phase) [32,33]. Since δ-phase has to play a crucial role during irradiation, its properties must be known. The study on properties like creep on δ-phase is scarce. Karahan and Buongiorno [14] reported that the value of $D_0$ and activation energy of δ-phase as $2 \times 10^{-7}$ m$^2$/s and 150 kJ/mol, respectively. However, there are many reports available in the literature about the creep behaviour of metal fuels. Some of the results are briefly given below.

The recommended creep rate correlation for U–Zr and U–Pu–Zr alloys is [17]:

$$\dot{\varepsilon} = 5 \times 10^3 \times (1 + 7.9 \times p + 470 \times p^2)\sigma \exp\{-52,000/RT\} + 6.0 \times (1 - p^{0.67})^{-0.8}\sigma^{4.5} \exp\{-52,000/RT\} + 7.7 \times 10^{-23} \times \sigma \times \dot{Y}. \quad (5)$$

where $\dot{\varepsilon}$ is the creep rate (s$^{-1}$), $p$ is the porosity expressed as a fraction of initial fuel volume, $R$ is the gas constant (1.987 cal/mol K), $\sigma$ is the stress (MPa), $T$ is temperature (K), $\dot{Y}$ is the fission rate (fissions/cm$^3$ s). Unlike ceramic fuel, metallic fuel retains sufficient fission gas to produce large volumes of fission gas bubbles at low burnup [34]. Bubbles can grow by creep through climb and glide of existing dislocations. The bubble radius $r$ is calculated using the classical solution for creep growth of a spherical cavity under pressure [35].

In the low temperature regime where creep is dominated by the deformation of the α uranium matrix, the creep rate is given by [40].

$$\dot{\varepsilon}(\mathrm{s}^{-1}) = (0.5 \times 10^4\sigma + 6.0\sigma^{4.5}) \exp(-26,170/T). \quad (6)$$

where $\sigma$ is in MPa. At higher temperatures, where the γ solid solution phase is formed, the creep rate is given by [40]:

$$\dot{\varepsilon}(\mathrm{s}^{-1}) = 8.0 \times 10^{-2}\sigma^3 \exp(-14,350/T). \quad (7)$$

It should be noted that the activation energies for creep in these two regimes are close to the activation energies for volume diffusion [36–38]. McDeavitt and Solomon [39] analyzed the results from hot isostatic pressing experiments performed on sintered hydride and metal-derived U–10 wt.% Zr (U–22.48 at.% Zr) samples. The phenomenon of HIP is related to grain boundary diffusion and creep cavitation mechanisms for cavity growth during creep [40]. It was found that the model of Chen and Argon [41] for HIP controlled by coupled grain boundary diffusion and power-law creep agreed best with the HIP behaviour of γ-phase U–10%Zr. The activation energy (187 ± 10 kJ/mol) agrees with a reported value for grain boundary diffusion of uranium in γ-U [39]. The measured HIP activation energy is significantly higher than the reported value for volume diffusion in γ-phase U–10%Zr (112 kJ/mol [39,42]), but is in agreement with the reported value for grain boundary diffusion of uranium in γ-phase uranium (187 kJ/mol [43]. The activation energy for volume diffusion in a U–Zr alloy containing between 5 and 10 wt.% Zr (12.07 and 22.48 at.% Zr) should be between 134 and 113 kJ/mol [42]. An approximate uniaxial creep expression data for U–10%Zr was generated [39]:

$$\dot{\varepsilon}(\mathrm{s}^{-1}) = 4 \times 10^{-10}\sigma^5. \quad (8)$$

where $\sigma$ is in units of MPa. With the above background in mind, we will analyze the creep behaviour of δ-phase made by arc-melting using impression creep technique.

It is generally accepted that the mechanical behaviour of metallic materials at homologous temperatures ($T/T_m$, where $T_m$ is the melting temperature) higher than 0.5 can be fairly expressed by the power-law creep over a wide range of strain rates [44–46]. Thus, for steady-state creep, the high temperature creep rate $\acute{\varepsilon}$ is often described by the well-known formula:

$$\acute{\varepsilon} = A\sigma^n \exp(-Q/RT). \quad (9)$$

where $\sigma$ is the applied stress, $A$ *is* a material parameter, $n$ denotes the stress exponent, $Q$ the activation energy, $T$ the temperature, and $R$ is the universal gas constant.

The value of activation energy for creep obtained for δ-phase in this study is 106 ± 4 kJ/mol. The value of activation energy reported by Karahan et al. for δ-phase is 150 kJ/mol, which is about 30% higher than the value reported in this study. The homogeneity range of the δ-phase was found to be 64.2–78.2 at.% Zr at 600 °C and 66.5–80.2 at.% Zr at 550 °C. The activation energy is reported to vary with Zr concentration in U–Zr system [47]. The value of activation energy obtained in this study matches with values of activation energy for diffusion of U in Zr for about 30 at.% Zr. A characteristic parameter describing the high temperature creep is the stress exponent, $n$, for steady-state creep rate in the power-law creep equation. The stress exponent obtained in this study hovers around 6–7. Several mechanisms have been proposed in the literature to account for the creep rate observed at high temperatures. Mechanism based on diffusional flow such as Herring-Nabarro creep and Coble creep can be straight away discounted since these models require "$n$" to be unity or nearly so. The observed values of $n$ are much higher. Two mechanisms have been mainly referred to in the literature which predict $n$ values in the experimental range of 4–7. These are: (i) the model of climb of edge dislocation [48,49] and (ii) the model of jogged screw dislocation motion [50]. The expected activation energy for creep is the same for the two mechanisms (namely the activation energy for self-diffusion). Hence, the mechanism of creep in this alloy is expected to be climb-controlled dislocation creep.

## 7. Conclusions

The creep behaviour of δ-phase of U–50%Zr alloy was studied using impression creep technique in the temperature range of 525–575 °C using different stress levels and the following conclusions are drawn:

1. The impression creep curves for δ-$UZr_2$ are similar to the conventional creep curves with steady state attained after an initial transient period.
2. A power law behaviour is displayed by all the alloys. The stress exponents range from 6.5 to 7.
3. The activation enthalpy for the δ-$UZr_2$ is independent of stress with an average value of 106 ± 4 kJ/mol.
4. Climb-controlled dislocation creep is considered to be the rate-controlling deformation mechanism for this alloy.

## References


[1] R.I. Sheldon, D.E. Peterson, in: T.B. Massalski et al. (Eds.), Binary Alloy Phase Diagrams, vol. 2, American Society for Metals, Metals Park, OH, 1986, p. 2150.
[2] H. Okamoto (Ed.), ASM Metals Handbook, Binary Alloy Phase Diagram, vol. 3, Updating Service, ASM International, 1992, p. 381 (Chapter 2).
[3] R.I. Sheldon, D.E. Peterson, Bull. Alloy Phase Diag. 10 (2) (1989) 165.
[4] M. Akabori, A. Itoh, T. Ogawa, F. Kobayashi, Y. Suzuki, J. Nucl. Mater. 188 (1992) 249.
[5] M. Akabori, A. Itoh, T. Ogawa, T. Ogata, J. Alloys Compds. 271–273 (1998) 597.
[6] T. Ogawa, T. Iwai, J. Less-Comm. Met. 170 (1991) 101.
[7] M. Akabori, T. Ogawa, A. Itoh, Y. Morii, J. Phys.: Condens. Matter. 7 (1995) 8249.
[8] J.M. Silcock, J. Met. 9 (1957) 521.
[9] T. Ogata, M. Akabori, A. Itoh, T. Ogawa, J. Nucl. Mater. 232 (1996) 125.
[10] Y. Adda, A. Kirianenko, J. Nucl. Mater. 6 (1962) 130.
[11] Douglas E. Burkes, Randall S. Fielding, Douglas L. Porter, Douglas C. Crawford, Mitchell K. Meyer, J. Nucl. Mater. 389 (2009) 458.
[12] G.L. Hofman, L.C. Walters, T.H. Bauer, Prog. Nucl. Energy 31 (1997) 83.
[13] G.L. Hofman, R.G. Pahl, C.E. Lahm, D.L. Porter, Metall. Trans. A 21A (1990) 517.
[14] A. Karahan, J. Buongiorno, J. Nucl. Mater. 396 (2010) 283.
[15] L. Leibowitz, R.A. Blomquist, A.D. Pelton, J. Nucl. Mater. 167 (1989) 76.
[16] G.L. Hofman, S.L. Hayes, M.C. Petri, J. Nucl. Mater. 227 (1995) 277.
[17] W.J. Carmack, D.L. Porter, Y.I. Chang, S.L. Hayes, M.K. Meyer, D.E. Burkes, C.B. Lee, T. Mizumo, F. Delage, J. Somers, J. Nucl. Mater. 392 (2009) 139.
[18] B. Cohen, H. Tsai, L.A. Neimark, J. Nucl. Mater. 204 (1993) 244.
[19] T.C. Hsieh, J. Rest, Modeling of Fuel/Fission-product Behavior, NUREG/CR-1691, 1980 (January–March).
[20] Y.S. Kim, S.L. Hayes, G.L. Hofman, A.M. Yacout, J. Nucl. Mater. 359 (2006) 17.
[21] D.H. Sastry, Mater. Sci. Eng. 409 (2005) 67.
[22] J.C.M. Li, Mater. Sci. Eng. A 322 (2002) 23.
[23] S.N.G. Chu, J.C.M. Li, Mater. Sci. Eng. 39 (1979) 1.
[24] S.N.G. Chu, J.C.M. Li, J. Mater. Sci. 12 (1977) 2200.
[25] E.C. Yu, J.C.M. Li, Philos. Mag. 36 (1977) 811.
[26] R.S. Sundar, T.R.G. Kutty, D.H. Sastry, Intermetallics 8 (2000) 427.
[27] G.S. Murthy, D.H. Sastry, Phys. Status Solidi 70 (1982) 63.
[28] G.S. Murthy, D.H. Sastry, Trans. Indian Inst. Met. 34 (3) (1981) 195.
[29] D.H. Sastry, G.S. Murthy, Trans. Indian Inst. Met. 39 (4) (1986) 369.
[30] Y. Adda, J. Philibert, H. Faraggi, Rev. Metall. 54 (1957) 597.
[31] Y. Adda, C. Mairy, J.L. Andreu, Rev. Metall. 57 (1960) 550.
[32] M. Ishida, T. Ogata, M. Kinoshita, Nucl. Technol. 104 (1993) 37.
[33] W. Hwang, B. Lee, J.Y. Kim, Ann. Nucl. Energy 27 (2000) 1059.
[34] L.C. Walters, B.R. Seidel, J.H. Kittel, Nucl. Technol. 65 (1984) 179.
[35] E.E. Gruber, J.M. Kramer, Gas bubble growth mechanisms in the analysis of metal fuel swelling, in: Proceedings of 13th International Symposium (Part-I) Radiation Induced Changes in Microstructure, ASTM-STP-955, 1987, p. 432.
[36] E.E. Gruber, The Role of Bubble-size Equilibration in the Transient Behavior of Fission Gas, USDOE Report ANL-78-36, 1978 (April).
[37] E.E. Gruber, J. Nucl. Mater. 110 (1982) 223.
[38] T. Ogata, T. Yokoo, Nucl. Technol. 128 (1999) 113.
[39] S.M. McDeavitt, A.A. Solomon, J. Nucl. Mater. 228 (1996) 184.
[40] S.M. McDeavitt, Hot Isostatic Pressing of U–10Zr Alloy Nuclear Fuel by Coupled Grain Boundary-diffusion and Power-law Creep, Ph.D. Thesis, Purdue University, 1992.
[41] I.W. Chen, A.S. Argon, Acta. Metall. 29 (1981) 1759.
[42] S.J. Rothman, Diffusion in Uranium and Its Alloys, Argonne National Laboratory Report ANL-5700 – Part C, 1961.
[43] I. Kaur, W. Gust, L. Kozma, Handbook of Grain and Interphase Boundary Diffusion Data, vol. 2, Ziegler, Stuttgart, 1989, p. 1345.
[44] I. Finnie, W.R. Heller, Creep of Engineering Materials, McGraw-Hill, New York, 1959.
[45] O.D. Sherby, P.M. Burke, Mechanical behavior of crystalline solids at elevated temperature, in: Progress in Materials Science, vol. 13, Pergamon Press, New York, 1967, pp. 325–390.
[46] H.A. Sailer, J.T. Stacy, N.S. Eddy, H.L. Klebanow, Creep Strength of Uranium Alloys at 1500 and 1600F, Battelle Memorial Institute Report BMI-834, 1953 (May 28).
[47] N.L. Peterson, WADD Technical Report 60-793, Wright Air Development Division, Wright–Patterson Air Force Base, Ohio, 1960 (March).
[48] J. Weertman, J. Appl. Phys. 26 (1955) 1213.
[49] J. Weertman, J. Appl. Phys. 28 (1957) 362, 1185.
[50] C.R. Barrett, W.D. Nix, Acta Metall. Mater. 13 (1965) 1247.